J Mater Sci: Mater Electron **(2024) 35:876**

Diffusion-enhanced efficiency of perovskite solar cells

Olavo Cardozo[3,6,*], Sajid Farooq[9], Aykut Kıymaz[2,7], Patricia M. A. Farias[8], Naum Fraidenraich[4], Andreas Stingl[3,5], Ricardo Maia-Junior[6], Severino Alves-Júnior[6], and Renato E. de Araujo[1]

[1] *Department of Electronic and Systems, Laboratory of Biomedical Optics and Imaging, Federal University of Pernambuco, Recife, PE 50732-970, Brazil*
[2] *Institute of Physical Chemistry and Linz Institute for Organic Solar Cells, Johannes Kepler Universität, 4040 Linz, Austria*
[3] *Phornano Holding GmbH, Kleineingersdorfer straße, 2100 Korneuburg, Austria*
[4] *Nuclear Energy Department, Federal University of Pernambuco, Recife, PE 50732-970, Brazil*
[5] *Phornano Brasil Ltda, Recife, PE 50010-360, Brazil*
[6] *Department of Fundamental Chemistry, Federal University of Pernambuco, Recife, PE 50740-560, Brazil*
[7] *Department of Mechanical Engineering, Ege University, 35100 Izmir, Turkey*
[8] *Department of Biophysics and Radiobiology, CB, Post Graduate Program on Material Sciences, CCEN, Federal University of Pernambuco, Recife, PE 50670-901, Brazil*
[9] *Center for Lasers and Applications, Instituto de Pesquisas Energéticas e Nucleares, IPEN-CNEN, São Paulo 05508-000, Brazil*

Received: 11 January 2024
Accepted: 5 April 2024
Published online: 29 April 2024

ABSTRACT

This study proposes a novel approach to improve the performance of third-generation solar cells, particularly perovskite solar cells (PSCs), by employing zinc oxide (ZnO) nanoparticles (NPs). The ZnO NPs are dispersed on the upper surface of the device, acting as nanodiffusers. This reduces reflection and increases solar radiation absorption in the photovoltaic active layer, enhancing the light pathway within the device. To analyze the impact of ZnO nanodiffusers on solar cell performance, computer simulations using the finite element method (FEM) and experimental analysis were conducted. Green synthesis methods were employed to synthesize ZnO nanoparticles with an average size of 160 nm, which were subsequently characterized. Thin films of ZnO NPs were deposited on the transparent indium tin oxide (ITO) electrode using spin coating, and their optical response was evaluated. This study proposes methodologies for optical and electrical modeling of third-generation photovoltaic cells using ZnO NPs. Optical computational modeling results evidence that ZnO nanospheres with a

Olavo Cardozo, Sajid Farooq, Aykut Kıymaz, Patricia M. A. Farias, Naum Fraidenraich, Andreas Stingl, Ricardo Maia-Junior, Severino Alves-Júnior, and Renato E. de Araujo have contributed to the study conception and design. The first draft of the manuscript was written by Olavo Cardozo and all authors commented on previous versions of the manuscript. All authors read and approved the final manuscript.

Address correspondence to E-mail: olavo.cardozo@ufpe.br

E-mail Addresses: sajiddahar@gmail.com; aykut.kiymaz@ege.edu.tr; patricia.mafarias@ufpe.br; naumfraiden2@gmail.com; andreas.stingl@phornano.com; ricardo.tadeu@ufpe.br; severino.alvesjr@ufpe.br; renato.earaujo@ufpe.br

https://doi.org/10.1007/s10854-024-12628-y

diameter of 160 nm predominantly scatter solar radiation in the forward direction. The incorporation of ZnO NPs (160 nm in diameter) reduces device reflectance, resulting in efficient light coupling and increased absorbance in the active layer. The integrated effects of light trapping and anti-reflective properties enhance photocurrent generation, leading to an increase in short-circuit current density. Experimental verification with ZnO NP deposition on PSCs confirms a 23.5% enhancement in photovoltaic device efficiency, increasing from 10.6 to 13.1% in an 11.68 cm^2 perovskite cell. The study presents the optical benefits of ZnO nanostructures, including anti-reflective effects and light scattering, when integrated into devices containing thin films as active material.

1 Introduction

The need for an efficient way to decrease greenhouse gas (GHG) concentrations in the atmosphere, in combination with the current geopolitical situation, accelerates the energy transition to renewables from fossil fuels. The use of photovoltaic devices contributes to the reduction of GHG emissions. Third-generation solar cells and, in particular, perovskite solar cells (PSCs) have proven to be a good candidate due to the low-cost materials and processes used for their manufacture, achieving the fastest increase in efficiency [1].

As a way to improve the efficiency of solar cells, especially thin films based, nanoparticles have been used in photovoltaic devices due to the possibility of "trapping" light and, thus, increasing the optical efficiency of the device. Through the use of nanostructures, it is possible to improve light absorption without increasing the thickness of the active layer, which would tend to generate more significant recombination between charge carriers [2].

Some researches showed that under diffuse radiation, in particular, organic and perovskite devices have demonstrated superior performance to Si devices [3–5]. Diffuse radiation involves light with different angles of incidence, which potentially adds new non-orthogonal light paths in the active layer with an extension longer than the thickness of the active layer [6–8], as shown in Fig. 1. The nanotextured surface of solar cells can increase the lengths of the optical path in the active material, mimicking diffuse radiation from a cloudy sky.

In this work, it is proposed to use ZnO nanodiffusers, produced from a green and scalable route on top of a perovskite thin film, to increase the power convertion efficiency of the device, reducing surface reflection and increasing the optical path in the active layer. It is important to note that ZnO nanostructures have also been used as electron transport layer in perovskite solar cells [9–11]. However, in this study, we analyze the influence of large ZnO nanostructures (160 nm diameter) that can promote optical enhancement of photovoltaic devices through the mechanism of light diffusion.

2 Methodology

2.1 Materials synthesis and characterization

A perovskite precursor solution was synthesized by mixing 461 mg of lead(II) iodide (PbI_2, 99%, Sigma-Aldrich) and 158 mg of Methyl-ammonium Iodide (CH_3NH_3I, 99%, Sigma-Aldrich), and dissolved in 1 mL of dimethylformamide (DMF), with molar ratio of 1:1 for CH_3NH_3I and PbI_2 precursors. The mixture

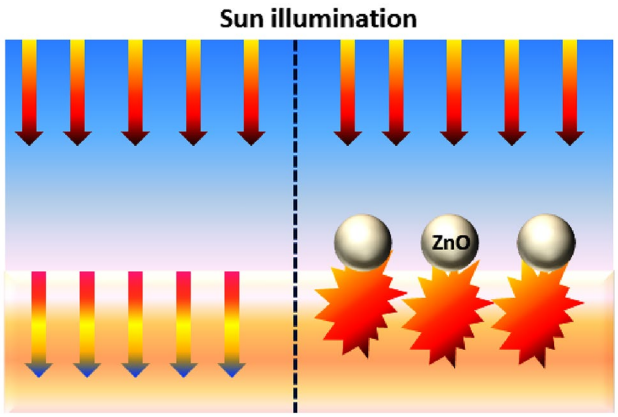

Fig. 1 Direct solar radiation with orthogonal pathways through the thin-film active medium (left half), and the generation of non-orthogonal pathways in active medium, induced by the nanodiffusors on the device surface (right half)

was kept in a stirrer to homogenization at 70 °C for 12 h.

The obtained XRD pattern (Fig. 7b) was acquired for a synthesized powder of perovskite ($CH_3NH_3PbI_3$). The powder is obtained by adding 1 mL of perovskite precursor solution, dropwise, in 4 mL of toluene in a penicillin glass, instantly forming a powder. Toluene was removed, and hexane was added to remove toluene excess. Hexane was removed, then the flask was put in vacuum oven for 20 min at 100 °C, so the powder can be dried.

A glass plate doped with indium tin oxide (ITO) (10 Ohm/sq) was cleaned by sonication with detergent in distilled water, acetone, and isopropyl alcohol for 20 min in each solvent. To make a perovskite film deposited on ITO glass. Then, 100 µL of the precursor solution was spread over the glass and spun in a spin coater at 2000 rpm for 18 s. The plate was annealed for 20 min at 110 °C. Despite the perovskite containing lead, a toxic material, the 200 nm thickness used does not pose significant risks, as the amount of lead present in the film is greatly reduced.

ZnO NPs were synthesized via the VERDEQUANT sol–gel method [12–14], as depicted in Fig. 2. In the synthesis process, gelatinization was obtained by applying whey, or a vegetal bio-compatible polymer, as a polymerization agent, resulting in a stable resin (xerogel), which was subsequently calcined at a temperature of 800 °C to obtain the ZnO nanoparticles. This synthesis route eliminates the need for fossil ethylene glycol and significantly reduces GHG emissions.

2.2 Computational modeling

The optical properties of ZnO NPs were investigated through computational simulations using the finite element method (FEM) and the radio-frequency (RF) module of COMSOL multiphysics. Simulation results provided absorption, scattering, and extinction cross-sectional spectra for the ZnO NPs. The simulation model considered a 160-nm-diameter nanosphere in the air as surrounding medium (this particle size has already been used by Cardozo et al. (2022), and predominantly induces frontal scattering, thus, reducing backward scattering). The interaction between the nanoparticle and a uniform plane wave was examined. The Albedo, defined as the ratio between the scattering and absorption cross sections of the ZnO NP, was analyzed, as well as the direction of light scattering [15]. Preliminary analyses employing Mie theory (considering the ZnO NP without a substrate) were conducted to validate the FEM simulation procedures.

To assess the impact of ZnO nanospheres on enhancing the performance of perovskite solar cells, a frequency-domain COMSOL model was created. The computational analysis accounts for the surface area occupied by ZnO nanoparticles (NPs) on the perovskite substrate. Based on the previous findings [15], an effective occupation area of 12.5% has been selected. This occupation area is defined as the ratio of the geometrical cross section of the NP to the surface area of the perovskite layer. The model incorporated a 160-nm-diameter ZnO nanosphere, representing a geometrical cross section ($A_g = \pi r^2$) of 2×10^{-14} m^2, positioned on the upper surface of a thin (200 nm) perovskite substrate, as shown in Fig. 3.

A linearly polarized plane wave was incident in the negative Z-direction. Perfect electric conductor (PEC) and perfect magnetic conductor (PMC) boundary conditions were applied perpendicular to the E and H fields, respectively, to simulate a periodic infinite array. To ensure a smooth modeling solution,

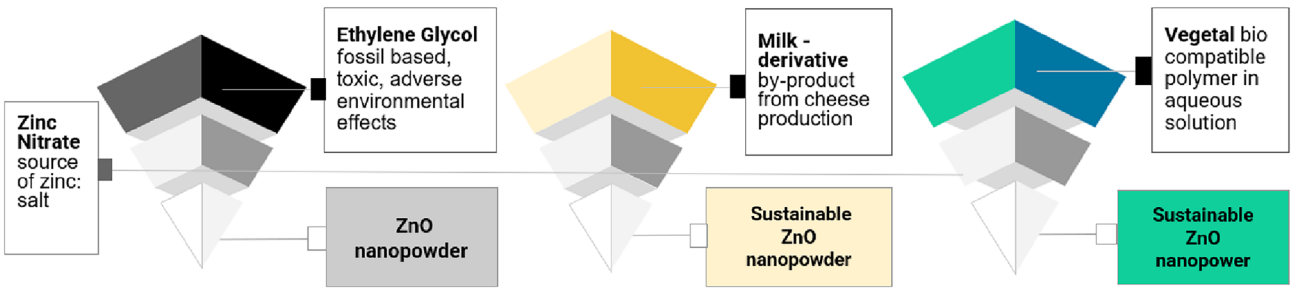

Fig. 2 ZnO synthesis route, from left to right: conventional, fossil reticulating agent based sol–gel synthesis, substituted firstly by a milk derivative and subsequently by a vegetal polymer in aqueous solution

the entire domain, including the nanostructure, was fully meshed. The absorbance (A), reflectance (R), and transmittance (T) values of the perovskite film were calculated both with and without a 160 nm ZnO NP on top. The model took into account previously reported refractive indices of MaPbI3 and ZnO [16, 17].

For assessing the performance of the photovoltaic platform consisting of a ZnO nanosphere on a perovskite substrate, the absorbed spectral irradiance (ASI) was defined as follows [15]:

$$\mathrm{ASI} = E_{\lambda}(\lambda) \times E_{s}(\lambda), \tag{1}$$

where E_{λ} represents the ASTM International G173 solar spectral irradiance with Air Mass 1.5, and $E_{s}(\lambda)$ denote the absorbance of the device. In addition, the platform absorption efficiency (AE) is defined as follows [18]:

$$\mathrm{AE} = \frac{\int_{\lambda_{\min}}^{\lambda_{\max}} \mathrm{ASI}\,\mathrm{d}\lambda}{\int_{\lambda_{\min}}^{\lambda_{\max}} E_{\lambda}\,\mathrm{d}\lambda}, \tag{2}$$

where the integration limits $\lambda_{\min}$ and $\lambda_{\max}$ were considered to be 400 nm and 900 nm, respectively.

To evaluate the impact of using the ZnO NP on the performance of the perovskite cell, the enhancement in absorption efficiency ($\mathrm{AE_{enh}}$) was defined as follows:

$$\mathrm{AE_{enh}} = \frac{\mathrm{AE_{NP}} - \mathrm{AE_{film}}}{\mathrm{AE_{film}}} \times 100, \tag{3}$$

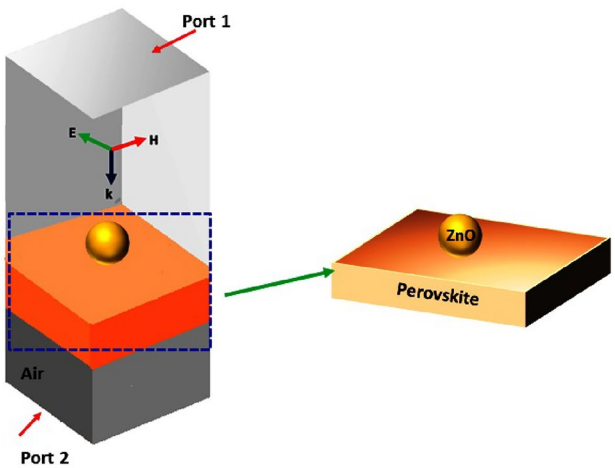

Fig. 3 Computational modeling framework for perovskite substrate with ZnO NP

where $\mathrm{AE_{film}}$ represents the absorption efficiency of the perovskite film (without NPs), and $\mathrm{AE_{NP}}$ is the absorption efficiency of the device covered by NPs.

To convert optical gain ($\mathrm{AE_{enh}}$) into electrical gain, an equivalent electrical circuit was explored [19]. Knowing that the J–V curve of a device can be considered as the dark curve (diode curve) plus a current source. It is possible to trace a new curve by modifying the intensity of the current source (converting the optical gain achieved into a proportional increase in the photogenerated current). This hypothesis is valid when the mean free path of the carriers in the active region is greater than the dimensions of that region [20].

2.3 Evaluation of absorption gain in the substrate

To assess the experimental absorption gain that a spin-coated film could provide in a thin film of photovoltaic material, such as perovskite ($CH_3NH_3PbI_3$), the experimental setup shown in Fig. 4 was employed. The process is based on measuring the absorbance of the photovoltaic film (S1), followed by measuring the absorbance of the ZnO film on a separate substrate (S2). Subsequently, the absorbance of both films combined was measured (S3). By subtracting ((S3)–(S2)), the remaining absorbance only originates from the photovoltaic film. The result of this subtraction will be compared with (S1). The measurements were conducted using an HR4000 UV-NIR spectrometer (Ocean Optics) and a DT-MINI-2 Deuterium Tungsten halogen light source (Ocean Optics).

2.4 Electrical evaluation of solar cell

Perovskite cells with inverted architecture (ITO/PEDOT:PSS/$MAPbI_3$/PCBM/TiO_2/Al) were fabricated. The solar cell is then encapsulated using epoxy resin. A glass plate was placed on the back side of the device to aid in its placement within the spin coater. Subsequently, a suspension containing ZnO NPs (previously sonicated) was carefully deposited onto the device's surface.

The electric assessment of the devices, both with and without the deposited nanostructures on their surfaces, involved evaluating current density versus

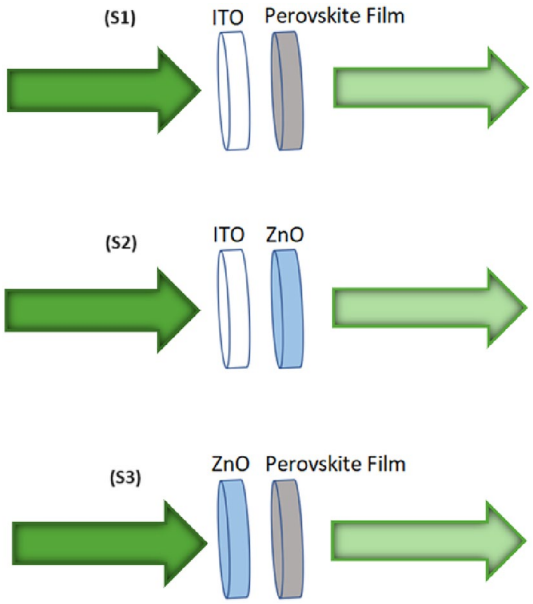

Fig. 4 Setup for optical experiments with ITO/perovskite layer and ZnO NPs/ITO/perovskite layer

voltage curves. Critical parameters such as V_{oc} (open-circuit voltage), J_{sc} (short-circuit current density), and *FF* (fill factor) were inferred from this analysis, which assesses the device's performance. The experiment setup is shown in Fig. 5.

3 Results and discussion

3.1 Synthesized materials characterization

High-resolution transmission electron microscopy (HR-TEM) analysis was conducted. Geometrical evaluation of 241 nanoparticles from 20 TEM images was performed to determine their size and shape. The TEM results revealed the formation of spherical nanoparticles with a Feret diameter of 163 nm (Std. Dev. = 71 nm). These nanoparticles exhibited a slight elongation, with an average aspect ratio of 1.25 (Std. Dev. = 0.23). Among the nanoparticles analyzed, the smallest Feret diameter measured was 125 nm (Std. Dev. = 51 nm).

Figure 6 depicts the analysis conducted using scanning electron microscopy (SEM) with ZnO nanostructures produced through the VERDEQUANT method. The SEM images reveal that the nanoparticles appear agglomerated, which can be attributed to the metallization process involved in the SEM analysis. The average size of the nanoparticles observed in the SEM analysis is consistent with the size determined by TEM analysis.

The crystalline structure of ZnO nanoparticles, prepared using the VERDEQUANT method, was analyzed using X-ray diffraction (XRD) as shown in Fig. 7a. The XRD peaks at angles (2θ) of 31.78°, 33.9°, 36.8°, 47.63°, 56.67°, 62.94°, 67.98°, and 69.1° correspond to the crystal planes [100], [002], [101],

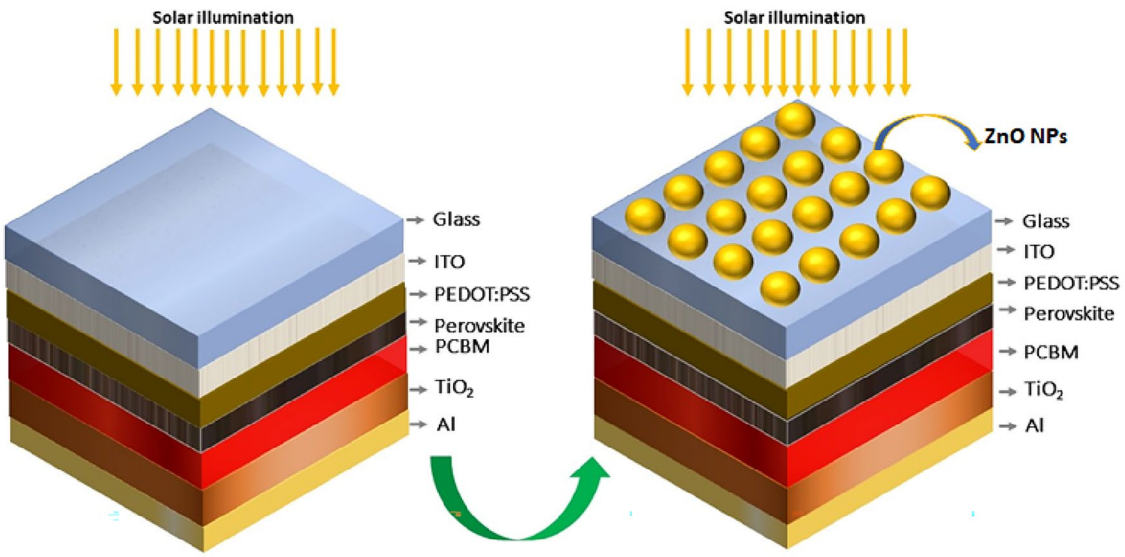

Fig. 5 Setup for electrical experiments with perovskite device and ZnO NPs/perovskite device

[102], [110], [103], [112], and [201] of the hexagonal wurtzite zinc oxide structure [21]. No characteristic peaks other than ZnO were observed.

The average grain size (D) of the ZnO nanoparticles was determined using the Scherrer's equation, given by [22]:

$$D = \frac{k\lambda}{\beta cos\theta}, \tag{4}$$

where K is a dimensionless shape factor, with a value close to unity (0.91 for most cases), also known as Scherrer's factor, λ is the X-ray wavelength (CuK_α = 0.15406 nm), β is the full width at half maximum intensity (FWHM) in radians, and θ is the Bragg's diffraction angle. Therefore, the ZnO nanoparticles have average diameter of 163 nm, which is according to image analysis.

Figure 7b presents the X-ray diffraction (XRD) characterization of the synthesized perovskite material. The XRD pattern reveals distinct diffraction peaks similar to the tetragonal unit cell, as explained by Baikie et al. (2013), with space group *I4/mcm* citeb74. Crystallographic planes can be indexed as (002), (110), (112), (200), (211), (202), (004), (220), (114), (222), (310), (204), (312), (224), (400), and (314), respectively corresponding to (2θ) angles: 13.97°, 14.10°, 19.91°, 20.00°, 23.48°, 24.48°, 28.16°, 28.43°, 31.63°, 31.81°, 31.87°, 34.79°, 34.96°, 40.45°, 40.65°, and 43.05°, resulting in these lattice parameters: $a = b = 8.87$ Å, $c = 12.66$ Å, $\alpha = \beta = \gamma = 90°$.

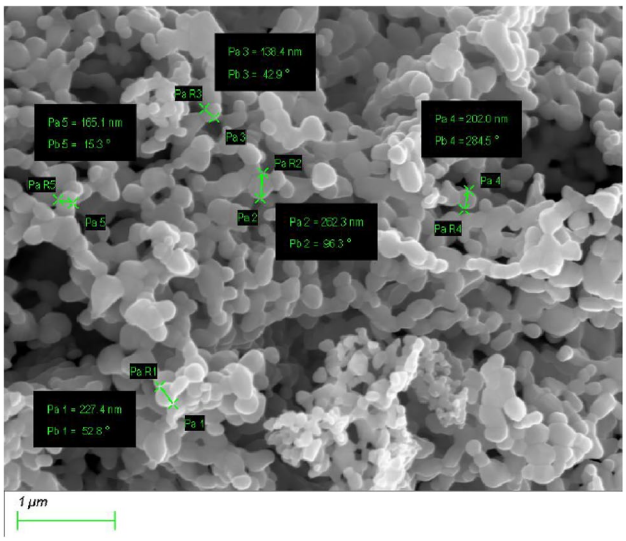

Fig. 6 SEM image of the synthesized ZnO NPs. (Courtesy of Dr. V. Dracopoulos and G. Voyiatzis at FORTH/ICE-HT-Greece, in the frame of DIAGONAL, supported by the European Union's H2020 R &I programme, Grant Agreement No. 953152)

3.2 Computational modeling

Computational simulations were conducted to evaluate the optical cross-sectional values of ZnO nanospheres with a diameter of 160 nm. Figure 8 illustrates the resulting theoretical spectra of absorption, scattering, and extinction cross sections for the ZnO nanoparticles, considering air as the surrounding medium and revealing that scattering dominates the

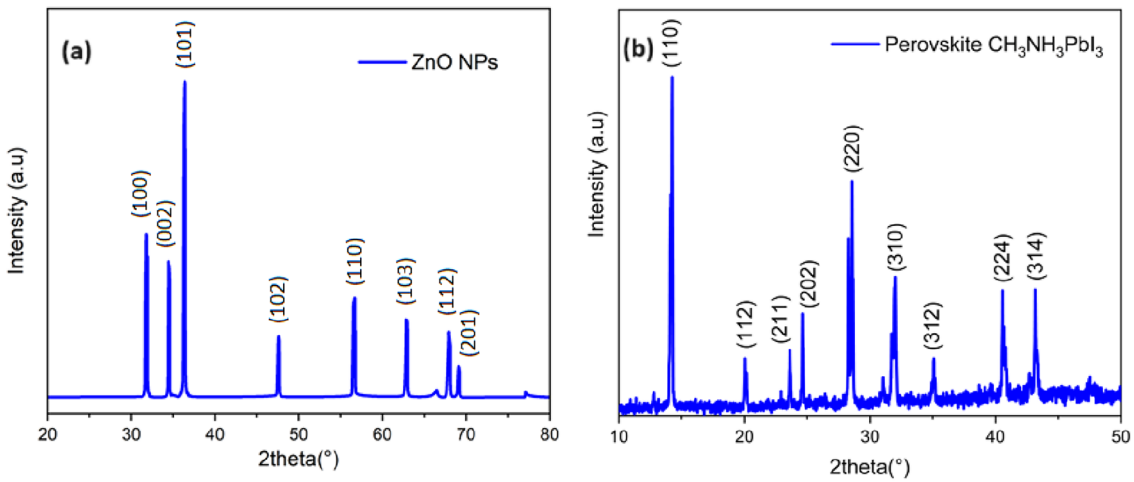

Fig. 7 **a** X-ray diffractogram obtained from synthesized ZnO NPs, with the typical pattern of crystalline wurtzite structure. **b** X-ray diffractogram of the synthesized perovskite powder

interaction between light and the ZnO nanoparticles. In the visible range, the contribution of absorption to the ZnO NP-light interaction is considered negligible. However, in the ultraviolet spectral region, where the photon energy exceeds the ZnO bandgap, both σ_{sca} and σ_{abs} exhibit comparable magnitudes. Furthermore, the extinction spectrum exhibits a prominent peak at 370 nm, which is a characteristic feature of ZnO nanospheres [24].

The inset of Fig. 8 shows the polar far-field scattering patterns of the 160 nm ZnO particle for visible wavelengths (400 nm, 500 nm, and 600 nm), revealing a high directionality (forward direction) of light scattered by 160 nm ZnO nanoparticles. Therefore, the use of ZnO nanoparticles on the surface of a solar cell could significantly enhance the light absorption within the device, leading to a decrease in device reflectance and ultimately improving its overall performance.

To assess the impact of ZnO NPs on the photovoltaic substrate, absorbance spectra were obtained through computational simulations. Figure 9 illustrates the absorbance spectra of the perovskite film with and without ZnO NPs for different incident angles, and considering an NP occupation area of 12.5%. The ZnO NPs scatters light, increasing the optical path inside the perovskite film and, therefore, enhancing the device absorbance for all angle of light incidence. This analysis provides valuable information for understanding the effects of ZnO NPs on the photovoltaic surface and their potential implications on the device's efficiency.

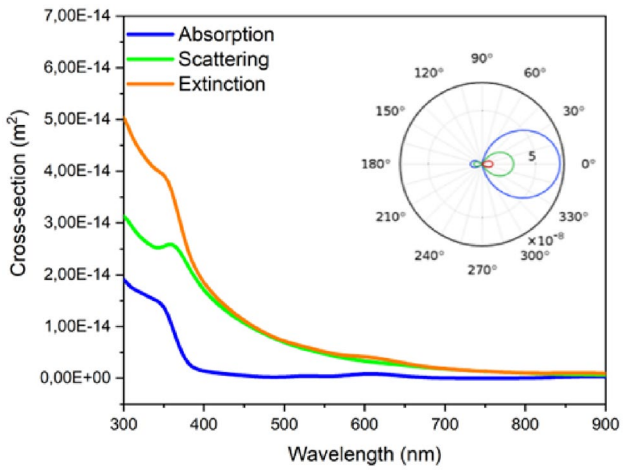

Fig. 8 Absorption, scattering, and extinction cross sections of 160 nm ZnO NP. *Inset* polar far-field scattering patterns of the 160 nm ZnO particle for visible wavelengths (400 nm, 500 nm, and 600 nm)

3.3 ZnO NPs deposition

On the deposition of ZnO NPs on a flat surface, the distribution of particles is reliant on the rotational speed and acceleration used on the spin-coating procedure.

Figure 10a depicts the absorbance of the spectrum of a glass slide with 163-nm-diameter ZnO nanoparticles deposited on the surface, using three different rotational speed (4000, 6000, 8000 rpm) and acceleration of 4000 rpm/s^2 on the spin-coating procedure. The high absorbance values obtained with 4000 rpm indicate that higher NP surface concentration is achieved with lower speeds.

Figure 10b depicts the transmittance spectrum of a glass substrate with ZnO nanoparticles deposited on top, as well as the transmittance of the glass alone. The graph indicates that the transmittance of the ZnO

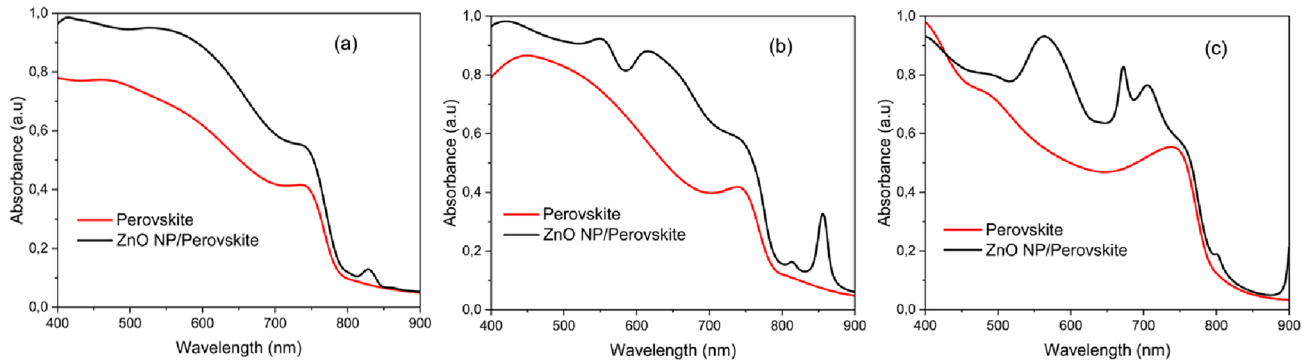

Fig. 9 Absorbance for 200-nm-thick perovskite substrate for different incidence angles, with and without ZnO NP on the top surface. **a** Normal incidence; **b** 30 degree incidence; **c** 45 degree incidence

NPs/glass combination is higher than that of the glass alone. This observation suggests a reduction in losses due to an anti-reflective effect caused by the presence of ZnO NPs.

A suspension containing ZnO nanoparticles in isopropanol (using a modified version of the Guiot and Spalla method [25]) was sonicated and subsequently deposited on ITO/glass through spin coating with 3000 rpm. A perovskite film was also deposited on ITO/glass. The absorption spectrum of ZnO NPs/Perovskite were obtained, accordingly to Sect. 2.3, as shown in Fig. 11.

There is an increase in absorption throughout the visible region, and the optical gain obtained, integrating across the entire region, amounts to 13%.

Figure 12 shows the spectral irradiance of the sun and the absorbed spectral irradiance (*ASI*) of the device (Eq. 1), with and without nanostructures on its surface. Depositing 163nm ZnO NPs on top of perovskite active layer, an enhancement of the *ASI* is observed for almost all visible spectrum regions.

By using Eqs. (2 and 3), an optical enhancement of 13 % was calculated about the perovskite film without the use of the film with ZnO NPs acting as nanodiffusers to increase the optical path within the perovskite film.

Knowing that the *J*–*V* curve can be considered the dark curve, extracted from the experimental curve of the perovskite device (obtained for standard test conditions radiation level of 1000 W/m^2 and module temperature of 25 °C and AM 1.5) without NPs attached, plus a current source, it is possible to calculate (Fig. 14, black curve) the curve of the module with the 160 nm ZnO NPs attached by modifying the intensity of the current source (with a 13% increase in absorbance). This hypothesis is valid when the mean-free path of carriers in the active region is greater than the dimensions of the region.

In Fig. 13, it is possible to observe, through scanning electron microscopy (SEM) image, the nanostructures of ZnO deposited onto a perovskite device.

The device performance was evaluated with a solar simulator after encapsulation without ZnO NPs and with ZnO NPs deposition. The characteristic curve for the device with (blue) and without (red) ZnO NPs on top can be seen in Fig. 14. The

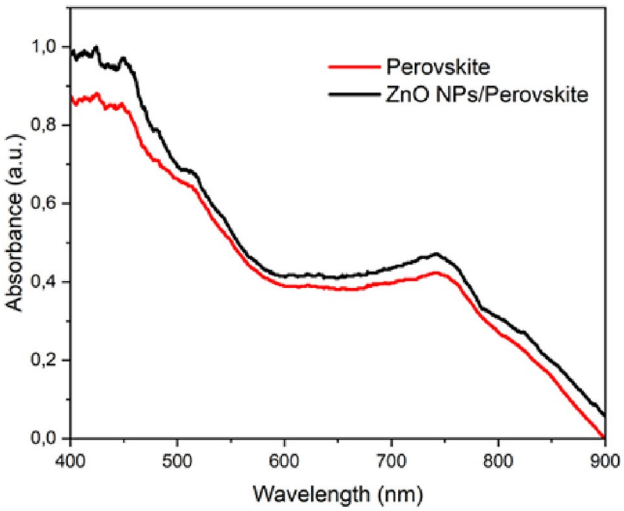

Fig. 11 Perovskite absorbance spectra, with (black) and without (red) 160nm ZnO NP on the top surface of the perovskite film

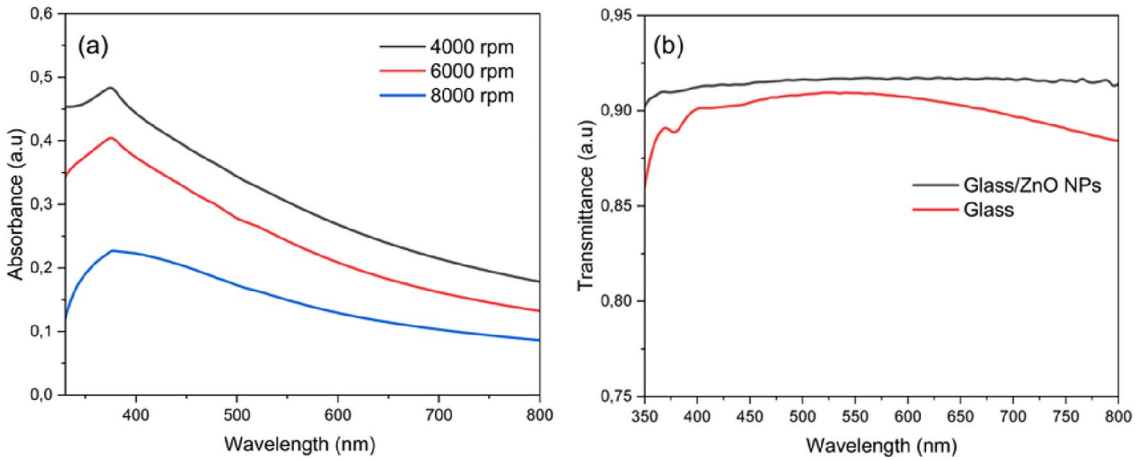

Fig. 10 **a** Absorption spectrum for thin films with ZnO NPs. **b** Transmittance for a glass substrate and the glass/ZnO NPs composition

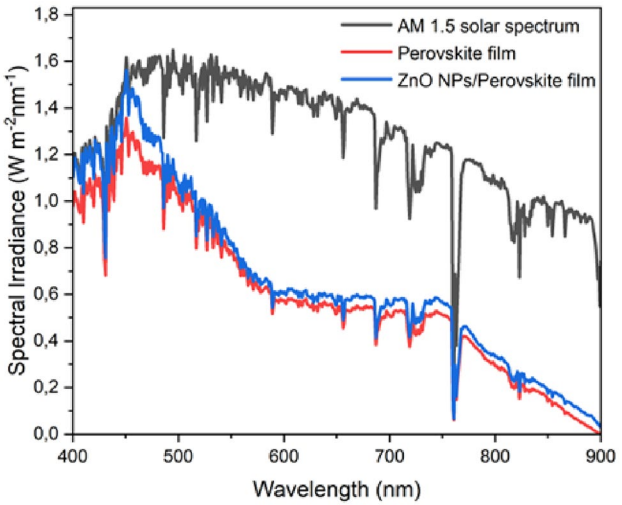

Fig. 12 Spectral absorption for a device with ZnO NPs on top (blue) and standard perovskite device (red)

curve generated considering an optical gain of 13% is shown in black (obtained through an experimental optical test, Fig. 12).

The parameters extracted from the *J*–*V* electrical curves for the standard device and the device with ZnO NPs deposited on top are represented in Table 1.

The use of ZnO nanoparticles as nanodiffusers has demonstrated a notable enhancement in current density, leading to an increase in power conversion efficiency of 23.5% increase in efficiency for the experimental result, while a 15% increase in efficiency was obtained for the modeling.

4 Conclusion

Despite some limitations of perovskite solar cells, such cells are recognized as promising for photovoltaic applications due to their low cost, module flexibility, and relative ease of large-scale production. As has been shown, the efficiency of these cells increases under diffuse radiation. Based on this finding, a biomimetic equivalent for the diffuse lighting of a cloudy sky, using"green" ZnO nanostructures, was proposed.

The results obtained through computer simulation demonstrated a gain of efficiency for perovskite solar cells using ZnO nanostructures deposited on top of the device, where ZnO nanoparticles dispersed in the upper surface of the cell could reduce reflection and increase solar absorption due to the increase of

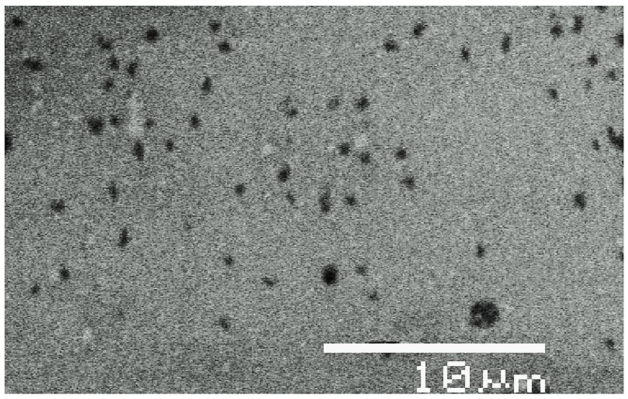

Fig. 13 SEM image for ZnO NPs on top of perovskite device

non-orthogonal light paths in the active layer of the device. The applied method to extract a curve in the dark from a characteristic curve (*J*–*V*) for a device and, from that dark curve, obtain a new *J*–*V* curve, considering an increase in the current source proportional to the obtained optical gain, proved to be effective.

After conducting the experimental work, it was confirmed that although zinc oxide is a popular and useful material in third-generation solar cells, distributing ZnO nanoparticles poses a difficulty. The formation of clusters and aggregation is not desirable for the production of thin-film cells, as they typically have a thickness ranging from 100 to 300 nm, and the presence of large particles could potentially damage the film's structure. For this reason, the most satisfactory application found for using ZnO nanomaterials would

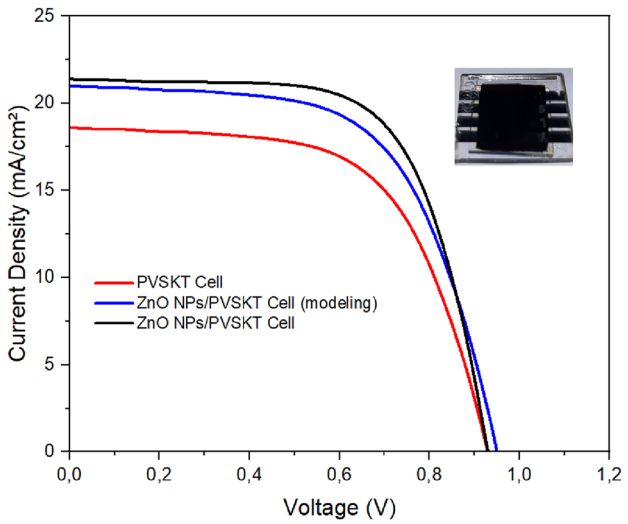

Fig. 14 Characteristic *J*–*V* curve for perovskite cell. Inset: Fabricated device

Table 1 Parameters extracted from the characteristic curves for the standard device, for the device with ZnO NPs deposited on top, and for the optical gain-based modeling

	Voc (V)	Jsc (mA/cm^2)	Vmp (V)	Jmp (mA/cm^2)	Ac (cm^2)	FF (%)	η (%)
PVSKT Cell	0.93	18.6	0.679	15.62	11.687	61.3	10.6
ZnO NPs/PVSKT Cell	0.93	21.42	0.68	19.4	11.687	66.2	13.1
ZnO NPs/PVSKT Cell (modeling)	0.95	21	0.679	18.02	11.687	61.3	12.2

be in the encapsulant used in such cells to promote an optical gain without harming the electronic properties of the device.

It has been experimentally demonstrated that glass with zinc oxide nanoparticles deposited on its surface transmits more light than just a glass substrate. It has been experimentally proved to be a gain through anti-reflective effect with ZnO nanoparticles. Furthermore, it was also demonstrated that thin films of perovskite ($CH_3NH_3PbI_3$) obtained optical gain (increase in the absorption of light) with the use of zinc oxide nanostructures. Finally, experimental tests were carried out in a solar simulator with encapsulated perovskite devices with deposited ZnO NPs in the encapsulating glass, and a gain of 23.5% in efficiency was obtained for the device with zinc oxide nanoparticles deposited on encapsulating glass.

Acknowledgements

The authors are grateful to Conselho Nacional de Desenvolvimento Científico e Tecnológico (CNPq), the National Institute of Science and Technology of Photonics (INCT de Fotônica), the Fundação de Amparo a Ciência e Tecnologia do Estado de Pernambuco (FACEPE) and the OeAD-GmbH. Austria's Agency for Education and Internationalisation. Aykut Kıymaz acknowledge to Scientific and Technical Research Council of Turkey (TÜBITAK) for financial support of A. KIYMAZ in the frame of program 2219 with the Grant No.: 1059B192201447. Mrs. Deniz Kıymaz is acknowledged for valuable comments on the experimental section of this paper. Professors Niyazi Sariciftci and Markus Scharber are gratefully acknowledged for accepting Olavo Cardozo and Aykut Kiymaz as visiting scientists in the Linz institute for organic solar cells (LIOS).

Funding

The authors declare that this project was partially supported by CAPES (Coordenação de Aperfeiçoamento de Pessoal de Nível Superior).

Data availability

The authors declare that they have availability of data and materials reported in this paper.

Code availability

The authors declare that they have availability of code reported in this paper.

Declarations

Conflict of interest The authors declare that they have no known competing financial interests or personal relationships that could have appeared to influence the work reported in this paper.

References

1. NREL, Best Research Cell Efficiencies. https://www.nrel.gov/pv/assets/images/efficiency-chart.png Accessed 04 Jan 2024
2. S. Jung, Y. Lee, J. Youn, H. Moon, J. Jang, J. Kim, Effect of the active-layer thickness on the short circuit current analyzed using the generalized transfer matrix method. J. Inf. Disp. **14**, 7–11 (2013)
3. C. Reynaud, R. Clerc, P. Lechêne, M. Hébert, A. Cazier, A. Arias, Evaluation of indoor photovoltaic power production

under directional and diffuse lighting conditions. Sol. Energy Mater. Sol. Cells **200**, 110010 (2019)
4. O. Cardozo, S. Farooq, A. Stingl, N. Fraidenraich, Investigation of performance of P3HT:PCBM organic photovoltaic module under real operating conditions. Sol. Energy **190**, 543–548 (2019)
5. A.B. Nikolskaia, S.S. Kozlov, M.F. Vildanova, O.I. Shevaleevskiy, Power conversion efficiencies of perovskite and dye-sensitized solar cells under various solar radiation intensities. Semiconductors **53**, 540–544 (2019)
6. M. Scharber, N. Sariciftci, Efficiency of bulk-heterojunction organic solar cells. Prog. Polym. Sci. **38**(12), 1929–1940 (2013)
7. L. Stevens, O. Höhn, M. Hanser, N. Tucher, C. Müller, S. Glunz, B. Bläsi, Impact of the refractive index on coupling structures for silicon solar cells. J. Photon. Energy **11**(2), 027001 (2021)
8. K. Li, S. Haque, A. Martins, E. Fortunato, R. Martins, M. Mendes, C. Schuster, Light trapping in solar cells: simple design rules to maximize absorption. Optica **7**, 1377–1384 (2020)
9. Z. Pang, Y. Sun, Y. Gao, X. Zhang, Y. Sun, J. Yang, F. Wang, L. Yang, Unravelling the mechanism of interface passivation engineering for achieving high-efficient ZnO-based planar perovskite solar cells. J. Power Sources **438**, 226957 (2019)
10. A.K.K. Kyaw, D.H. Wang, D. Wynands, J. Zhang, T.Q. Nguyen, G.C. Bazan, A.J. Heeger, Improved light harvesting and improved efficiency by insertion of an optical spacer (ZnO) in solution-processed small-molecule solar cells. Nano Lett. **13**(8), 3796–3801 (2013)
11. C. Li, C. Han, Y. Zhang, Z. Zang, M. Wang, X. Tang, J. Du, Enhanced photoresponse of self-powered perovskite photodetector based on ZnO nanoparticles decorated $CsPbBr_3$ films. Sol. Energy Mater. Sol. Cells **172**, 341–346 (2017)
12. A. Stingl, M. Silva, V. Alves, C. Ayala, E. Rodrigues, Method of producing a metal or metal oxide nanoparticle (WO2021046586). (2021). https://worldwide.espacenet.com/patent/search/family/072355731/ publication/WO2021046586A1?q=phornano
13. Phornano, Verdequant, Zinc Oxide. https://www.phornano.com/verdequant Accessed 15 Dec 2023
14. E.S. Rodrigues, M.S. Silva, W.M. Azevedo, S. Feitosa, A. Stingl, P.M.A. Farias, ZnO nanoparticles with tunable bandgap obtained by modified Pechini method. Appl. Phys. A **125**, 504 (2019)
15. O. Cardozo, S. Farooq, P.M. Farias, N. Fraidenraich, A. Stingl, R.E.D. Araujo, Zinc oxide nanodiffusers to enhance p3ht: pcbm organic solar cells performance. J. Mater. Sci. **33**(6), 3225–3236 (2022)
16. C. Stelling, C.R. Singh, M. Karg, T.A.F. König, M. Thelakkat, M. Retsch, Plasmonic nanomeshes: their ambivalent role as transparent electrodes in organic solar cells. Sci. Rep. **7**, 42530 (2017)
17. L.J. Phillips, A.M. Rashed, R.E. Treharne, J. Kay, P. Yates, I.Z. Mitrovic, A. Weerakkody, S. Hall, K. Durose, Dispersion relation data for methylammonium lead triiodide perovskite deposited on a (100) silicon wafer using a two-step vapour-phase reaction process. Data Brief **5**, 926–928 (2015)
18. S. Farooq, C.V.P. Vital, L.A. Gómez-Malagón, R.E. Araujo, D. Rativa, Thermo-optical performance of iron-doped gold nanoshells-based nanofluid on direct absorption solar collectors. Sol. Energy **208**, 1181–1188 (2020)
19. J. Cubas, S. Pindado, C. De Manuel, Explicit expressions for solar panel equivalent circuit parameters based on analytical formulation and the Lambert W-function. Energies **7**(7), 4098–4115 (2014)
20. W. Tress, *Organic Solar Cells Organic Solar Cells*, Springer Series in Materials Science, vol. 208. (Springer, Cham, 2014), p.139
21. A. Khorsand Zak, R. Razali, W.H.B. Abd Majid, M. Darroudi, Synthesis and characterization of a narrow size distribution of zinc oxide nanoparticles. Int. J. Nanomed. **6**, 1399–1403 (2011)
22. M. Farooqi, R. Srivastava, Enhanced UV–Vis photoconductivity and photoluminescence by doping of samarium in ZnO nanostructures synthesized by solid state reaction method. Optik **127**, 3991–3998 (2016)
23. T. Baikie, Y. Fang, J.M. Kadro, M. Schreyer, F. Wei, S.G. Mhaisalkar, M. Graetzel, T.J. White, Synthesis and crystal chemistry of the hybrid perovskite (CH_3NH_3) PbI_3 for solid-state sensitised solar cell applications. J. Mater. Chem. A **1**(18), 5628–5641 (2013)
24. F.R. Lamastra, M.L. Grilli, G. Leahu, A. Belardini, R. Li Voti, C. Sibilia, D. Salvatori, I. Cacciotti, F. Nanni, Photoacoustic spectroscopy investigation of zinc oxide/diatom frustules hybrid powders. Int. J. Thermophys. **39**, 110 (2018)
25. C. Guiot, O. Spalla, Stabilization of TiO_2 nanoparticles in complex medium through a pH adjustment protocol. Environ. Sci. Technol. **47**, 1057–1064 (2013)